ACS APPLIED MATERIALS & INTERFACES

Research Article

www.acsami.org

Modified Graphene/Polyimide Nanocomposites: Reinforcing and Tribological Effects

Ting Huang,[†] Yuanshi Xin,[†] Tongsheng Li,*[,†] Steven Nutt,[‡] Chao Su,[†] Haiming Chen,[†] Pei Liu,[†] and Zuliang Lai[†]

[†]State Key Laboratory of Molecular Engineering of Polymers, Department of Macromolecular Science, Fudan University, Shanghai, 200433, P. R. China

[‡]Department of Chemical Engineering and Materials Science, University of Southern California, Los Angeles, California 90089-0241, United States

Supporting Information

ABSTRACT: By taking advantage of design and construction of strong graphene−matrix interfaces, we have prepared modified graphene/polyimide (MG/PI) nanocomposites via a two-stage process consisting of (a) surface modification of graphene and (b) *in situ* polymerization. The 2 wt % MG/PI nanocomposites exhibited a 20-fold increase in wear resistance and a 12% reduction in friction coefficient, constituting a potential breakthrough for future tribological application. Simultaneously, MG also enhanced thermal stability, electrical conductivity, and mechanical properties, including tensile strength, Young's modulus, storage modulus, and microhardness. Excellent thermal stability and compatibility of interface, strong covalent adhesion interaction and mechanical interlocking at the interface, as well as homogeneous and oriented dispersion of MG were achieved here, contributing to the enhanced properties observed here. The superior wear resistance is ascribed to (a) tribological effect of MG, including suppression effect of MG in the generation of wear debris and protective effect of MG against the friction force, and (b) the increase in mechanical properties. In light of the relatively low cost and the unique properties of graphene, the results of this study highlight a pathway to expand the engineering applications of graphene and solve wear-related mechanical failures of polymer parts.

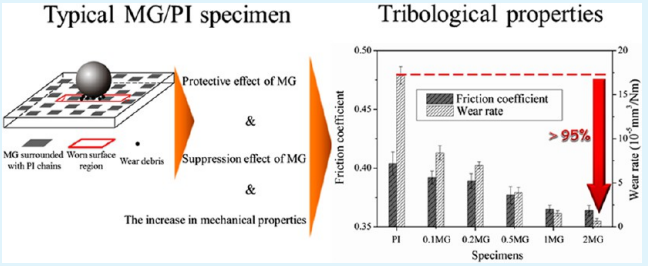

KEYWORDS: *modified graphene, polyimide nanocomposites, reinforcing effect, tribological effect, design and construction of interface*

1. INTRODUCTION

Graphene is a one-atom-thick planar sheet of sp^2-bonded carbon atoms arranged in a hexagonal lattice. Graphene may be the most important material of the next 20 years because of unique properties not manifested in any other single material.[1−5] More importantly, unlike carbon nanotubes (CNTs), graphene can be easily produced in large quantities from a graphite precursor, an important attribute for use as a filler additive. Indeed, graphene nanocomposites have been produced with various polymer matrixes, including epoxy,[6] nylon 12,[7] hydrogels,[8] polycarbonate,[9] polylactic acid,[10] polypropylene,[11] polyimide (PI),[12] poly(methyl methacrylate),[13] polyurethane,[14] and polystyrene.[15] Published studies such as those cited have demonstrated that graphene fillers can significantly enhance matrix properties, generating increased academic and industrial interest in the graphene-based polymer nanocomposites.

Aromatic PI exhibits a series of excellent physical and chemical properties, including thermal and thermo-oxidative stability, flexibility, solvent resistance, and superior mechanical, tribological, and electrical properties. Consequently, PI finds applications in automotive and transportation applications as well as in the aerospace industry, where it is often used for structural components.[12,16−19] Various nanoparticles has been employed to obtain high-performance PI nanocomposites for demanding service applications. For example, nanosilica enhanced the glass transition temperature (T_g) and reduced the coefficient of thermal expansion in the prepared hybrid PI film nanocomposites.[20] Likewise, the incorporation of modified multiwalled carbon nanotubes (MWCNTs) improved the tensile strength and modulus of MWCNTs/PI nanocomposites.[21] The addition of single-walled carbon nanotubes (SWCNTs) yielded a 2-fold increase in the wear life of nanocomposite films.[19] Until recently, the attention of numerous researches has turned to graphene. Yoonessi and co-workers have reported that the addition of graphene can improve the recovery rate of shape memory graphene/PI nanocomposites.[12]

The property enhancement of nanofiller reinforced polymer nanocomposites depends on the interface adhesion strength,

Received: February 19, 2013
Accepted: May 14, 2013
Published: May 14, 2013

   dx.doi.org/10.1021/am400635x | ACS Appl. Mater. Interfaces 2013, 5, 4878−4891

filler nature, filler dispersion and distribution, and the spacing between filler particles.[22−25] Functionalization of CNTs can be employed to achieve homogeneous dispersion in the matrix, yielding high-quality polymeric carbon nanocomposites.[26] For example, complexed SWCNTs/PI nanocomposites exhibited increases of 28 °C in T_g and a 20-fold in storage modulus.[27] Likewise, covalently bonded layered silicates/PI nanocomposites exhibited an increase of up to 36 °C in the degradation temperature and a reduction of up to 54% in moisture absorption.[28] Furthermore, modulus values of the imidized graphene/PI nanocomposites were 25−30% greater than those of unmodified graphene/PI nanocomposites.[12] These studies demonstrate that achieving performance enhancements in polymer nanocomposites requires control of filler dispersion and careful engineering of interfaces by modification of filler surfaces.

Presently, significant barriers prevent the widespread use of advanced materials solutions for minimizing friction and wear-related mechanical failures.[29,30] Since graphene was first reported as a free-standing nanoparticle by Geim and co-workers,[1] studies of the tribological properties of graphene have focused primarily on the nano- and microscale aspects.[22−24,31−35] The relationship between tribological and other properties awaits systematic and comprehensive study.[36−42] For the macroscale tribological aspect, oil with α-Fe_2O_3 nanorod/graphene oxide (GO) composites showed superior tribological properties compared to neat oil.[37] However, earlier tribological studies showed that the incorporation of unmodified GO into polymer matrix, such as nylon,[38] PI,[39] ultrahigh molecular weight polyethylene,[40] nitrile rubber,[41] and poly(ether ether ketone),[42] enhanced wear resistance far less than expected. Moreover, the addition of GO in some cases increased the friction coefficient and wear rate.[39,40] Nevertheless, from the references cited above, graphene could be deployed as a wear-resistant filler through intelligent control of both dispersion and interface structure/chemistry. However, further efforts are required to demonstrate design pathways to macroscale tribological performance of graphene nanocomposites and to explore more deeply the mechanisms responsible for the structure−property relationships.

In the present work, we describe our efforts to design and construct strong interfaces in the graphene/PI nanocomposites via (a) covalent grafting of small molecule segments (SMS) containing amino groups (NH_2) onto a chemically reduced graphene (GN) surface, (b) preparation of modified graphene/polyimide (MG/PI) nanocomposites by *in situ* polymerization. The MG/PI nanocomposites exhibited increased mechanical properties, thermal stability, electrical conductivity, and tribological properties, particularly a 20-fold increase in wear resistance. We investigated the essential factors and mechanisms responsible for the observed mechanical and tribological properties and attempted to determine the relationship between mechanical and tribological properties.

2. EXPERIMENTAL SECTION

2.1. Materials. Expandable graphite (EG) powders (Yingtai Co., Yangtai, China) and bisphenol A dianhydride (BPADA, Shanghai Research Institute of Synthetic Resins, Shanghai, China) were selected and acquired. In addition, 4,4′-diphenylmethane diisocyanate (MDI), isopentyl nitrite, sodium dodecylbenzene sulfonate (SDBS), and 2-(4-aminophenyl) ethanol were acquired from Aladdin Reagent Co., Shanghai, China. 4,4′-Oxydianiline (4,4′-ODA), *N*,*N* -dimethylformamide (DMF), and 50% hydrazine hydrate were provided by Sinopharm Group Chemical Reagent Co., Ltd., Shanghai, China.

2.2. Preparation of SMS-Modified Graphene (MG). GO was prepared from EG powders using a modified Hummers method, as reported elsewhere.[11,39] The detailed operation for covalent modification of GN with SMS containing amino groups can be described as follows: 100 mg of GO was redispersed in 200 mL of deionized water with the assistance of sonication at room temperature (RT). Then 2 g of SDBS and 0.6 mL of 50% hydrazine hydrate were added into the GO suspension, respectively. Subsequently, the mixture was stirred in an oil bath at 85 °C for 18 h, yielding the GN suspension. Afterward, 5 g of 2-(4-aminophenyl) ethanol and 3 mL of isopentyl nitrite were added into the above suspension. After stirring vigorously at 80 °C for 3 h, the mixture was filtered with a 0.2 μm Teflon filter film. To remove unreacted molecules, the collected powders were washed with DMF and deionized water until the filtrate was clear. Then the resulting black solids were vacuum-dried overnight at 70 °C, yielding GN−OH. The obtained GN−OH was redispersed in 300 mL of anhydrous DMF with the aid of sonication. In total, 2.503 g of MDI was added into the above suspension and the mixture was kept under vigorous stirring at 80 °C for 2 h under nitrogen. After washing three times with anhydrous DMF to remove the unreacted organics, the resulting solids (GN-MDI) were redispersed in 300 mL of anhydrous DMF with sonication. In total, 10.012 g of 4,4′-ODA was added and continued to stir overnight at 60 °C. The powders were collected by vacuum filtration and purified with excess DMF three times. Finally, the black solids were dried at 70 °C under vacuum overnight, yielding MG. Note that the last filtrate is free of unreacted organics by Fourier transform infrared (FTIR) analysis.

2.3. Preparation of MG/PI Nanocomposites. In a typical operation, 40 mg of MG was redispersed in 32 g of anhydrous DMF with the aid of sonication for 2 h at RT. A 150 mL three-necked flask was charged with the above suspension, 2.189 g of ODA and 5.809 g of BPADA, and then the mixture was stirred vigorously at RT for 24 h under nitrogen, yielding modified graphene/polyamide acid (MG/PAA) solution. To prepare MG/PAA solutions with different MG loadings, different quantities of MG were added to 32 g of anhydrous DMF. The final solid content of MG/PAA solution was 20%. The obtained MG/PAA solutions were kept in a freezer until use. The film specimens were fabricated using a solution casting method. The films on glass substrates were placed in a vacuum oven at RT to remove air bubbles and then were heated at 70 °C for 2 h and 100, 150, 200, and 300 °C for 1 h to completely get rid of volatile and achieve thermal imidization. The film thickness was ∼50 μm. The specimens for friction and wear tests were prepared by casting MG/PAA solutions onto a stainless steel plate. The detailed preparation for friction specimens can be found in our previous published work.[17] The MG/PI specimens (0.1 wt % MG/PI, 0.2 wt % MG/PI, 0.5 wt % MG/PI, 1 wt % MG/PI, 2 wt % MG/PI) containing 0.1 wt %, 0.2 wt %, 0.5 wt %, 1 wt %, and 2 wt % of MG were prepared by the above-mentioned experimental steps. Because of poor dispersion and obvious precipitation of 0.32 g of MG in 32 g of DMF, the 4 wt % MG/PI specimen was not prepared. For comparison, the neat PI and 1 wt % GN/PI specimens were fabricated in the same manner.

2.4. Friction and Wear Tests. The tribological tests were conducted on a reciprocating friction and wear testing machine (HS-2M, Lanzhou Zhongke Kaihua Technology Development Co., Ltd.). The contact schematic diagram of the frictional couple is shown (Supporting Information, Figure S1). The detailed friction test conditions, such as properties of the stainless ball, temperature, relative humidity, reciprocating frequency, applied load, length of stroke and time, were carried out according to our previous publication.[17] The friction coefficient was obtained by the computer automatically. At the end of each test, the depth of the wear scar was measured with a stylus surface profiler (Dektak 150, Veeco Instruments Inc.), and the wear volume (ΔV, mm^3) of the specimen was calculated according to the following equation:

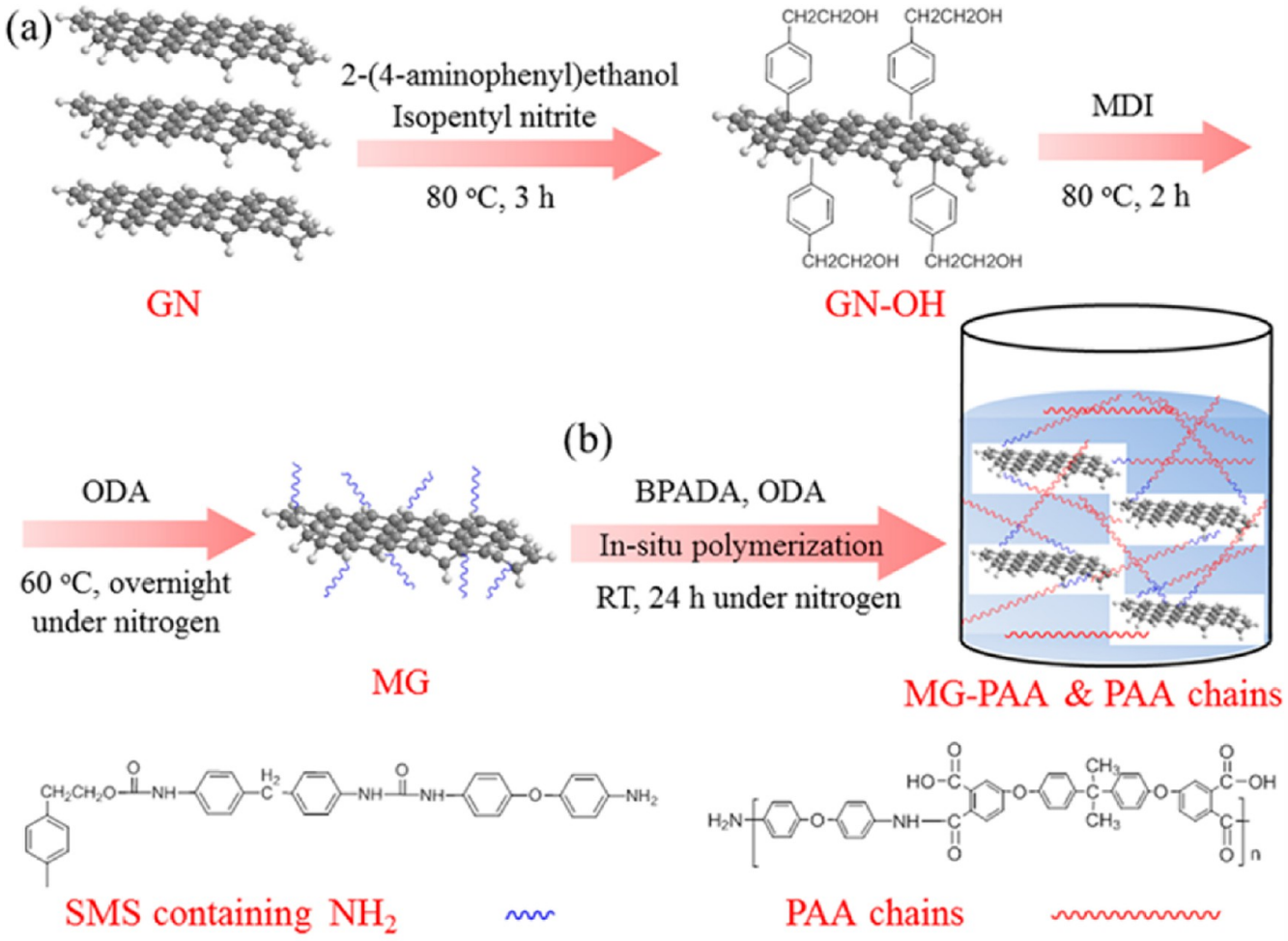

Figure 1. (a) Surface modification of GN with SMS containing NH_2 and (b) preparation of MG/PAA solutions via *in situ* polymerization.

$$\Delta V = \frac{L}{2}\left[r^2 \arccos\frac{r-d}{r} - (r-d)\sqrt{r^2-(r-d)^2}\right] + 2\int_0^d \pi\sqrt{r^2-(r-d)^2}\, d\left(\sqrt{r^2-(r-d)^2}\right) \quad (1)$$

where ΔV is the wear volume (mm^3), d the depth of the specimen (mm), L the length of stroke in one cycle (mm), and r the radius of the counterpart ring (mm). The wear rate (K, $mm^3/N\ m$) of the specimen was calculated from the following equation:

$$K = \frac{\Delta V}{FtvL} \quad (2)$$

where F is the applied load (N), t the experimental duration (s), v the reciprocating frequency (Hz), and L the stroke length in one cycle (m). In this work, five replicates of friction and wear tests were carried out to minimize data scattering, and the average results were reported in this article.

2.5. Characterization. Atomic force micrographs (AFM) were conducted using a commercial instrument (Digital Instruments Nano IV) in the tapping mode. FTIR spectra were recorded using a spectrometer (Nicolet Nexus 470). Thermogravimetric analyses (TGA) were carried out with Perkin-Elmer thermal analyzer under nitrogen flow at a heating rate of 20 °C min^{-1}. Raman spectra were collected on a Renishaw Invia Reflex micro-Raman spectrometer with 631 nm laser excitation. X-ray diffraction (XRD) patterns were acquired by a Panalytical X'pert diffractometer using Cu Kα radiation (λ = 0.154 nm) at an accelerating voltage of 40 kV and current of 40 mA. Dynamic mechanical analyses (DMA) were performed on a Netzsch DMA242 analyzer. All the specimens were performed under a tension mode from 100 to 300 °C at a heating rate of 5 °C min^{-1} and a frequency of 1 Hz, vibration amplitude being set to 120 μm, and static compressive stress of 4 N. The mechanical properties were measured using a universal testing machine (CMT-4102, Sans Co., China) for dumbbell-type specimens, according to ISO 527-3:1995 standard. The data reported here represented the average of five tests. Scanning electron microscopy (SEM) images of tensile fractured surfaces were observed on a Tescan 5136 MM SEM. The electrical conductivity of all the specimens was measured on a Keithley 2400 picoammeter using a standard four-probe method at RT. In order to investigate related tribological mechanisms, the morphologies of worn surfaces and debris were also observed by using SEM. Thin sections for field emission scanning electron microscopy (FESEM) observations were cut from the as-prepared nanocomposite films under cryogenic conditions using a Leica ultramicrotome with a diamond knife, and FESEM images were carried out by a Hitachi S-4800 FESEM to observe the distribution of filler in the PI matrix. Nanoindentation tests were conducted with an ultra nanoindentation tester (CSM Instruments, Switzerland) using a Berkovich diamond indenter. After contacting with the surface, the indenter was approached into friction specimens with a constant strain rate of 0.05 s^{-1} until 2000 nm of depth was reached, held at the maximum load for 50 s, and then withdrawn from the surface with the same rate as loading. At least five indents were performed on each specimen, and the average value was finally reported here. The micohardness was calculated by the Oliver and Pharr method.[43,44]

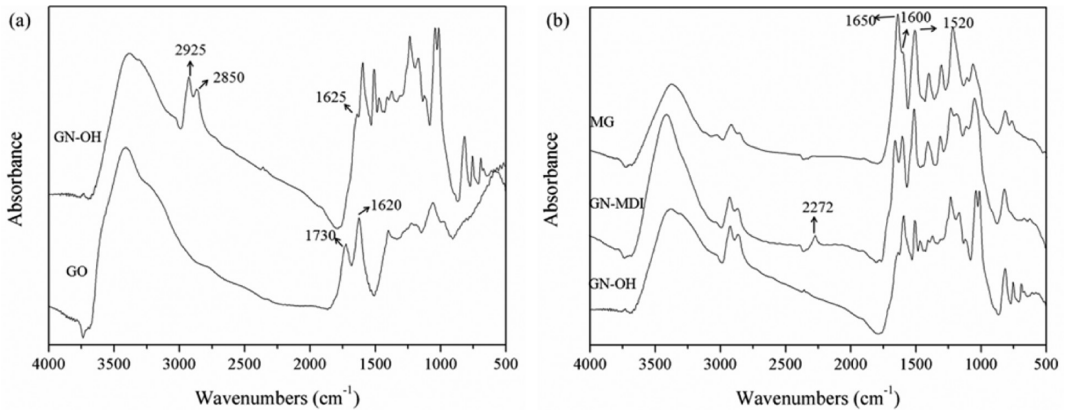

Figure 2. Structure characterization of as-prepared products: (a) FTIR spectra of GO and GN-OH and (b) FTIR spectra of GN-OH, GN-MDI, and MG.

3. RESULTS AND DISCUSSION

3.1. Surface Modification of GN with SMS. From the theoretical point of view of grafting-from methods, the notable steric hindrance effect of graphene should not be neglected due to the huge dimensions. In addition, the elimination of oxygenated groups would make GN tend to aggregate more readily in DMF solution.[5,22−25] It is expected that ideal SMS containing NH_2 can be grafted onto the GN surface (Figure 1a). This strategy aims at reducing the steric hindrance effect, affording homogeneous and stable dispersion of MG in DMF, increasing probability of engagement between grafted polymer chains and MG, and constructing excellent compatibility and thermal stability of the interface. MG affords a versatile starting platform for *in situ* fabrication of nanocomposites by grafting PAA at reactive sites (Figure 1b). More importantly, the preservation of a stable interfacial layer during thermal imidization is important for promoting interface adhesion and homogeneous dispersion, qualities that are necessary for efficient stress transfer.

The schematic procedure for surface modification of GN is depicted in Figure 1a. This process includes (1) grafting of 2-(4-aminophenyl) ethanol onto the GN surface, yielding functionalized graphene (GN−OH); (2) immobilization of MDI onto the GN-OH surface, preparing intermediate (GN-MDI); (3) immobilization of ODA onto the GN-MDI surface, yielding MG.

Figure 2 shows an FTIR spectral comparison that demonstrates the successful surface modification of GO. The two characteristic bands at 1730 and 1620 cm^{-1} for GO correspond to C═O and C═C stretching vibrations in the carboxyl and skeleton, respectively. After chemical reduction and diazonium addition, new absorptions arise from the introduction of phenylethanol groups onto the GN surface (Figure 2a). For example, the doublet at 2925 and 2850 cm^{-1} is assigned to the asymmetric C−H stretch of methylene groups in phenylethanol groups. Furthermore, the appearance of the characteristic band at 1625 cm^{-1} (−OH bending vibration of hydroxyl) provides definitive evidence for diazonium addition.

In comparison with GN-OH, GN-MDI shows new bands (Figure 2b) at 1650 cm^{-1} (C═O stretching vibration of amide carboxyl) and 1520 cm^{-1} (N−H bending vibration of amide), indicating that MDI has been covalently grafted onto the GN-OH surface. As expected, the band at 2272 cm^{-1} (isocyanate groups) persists in the spectrum of GN-MDI. It can be inferred that the other isocyanate group of MDI was retained for further reaction. By the incorporation of ODA, the band of the isocyanate group disappears completely (Figure 2b), whereas the intensity of the amide I and II bands increases (the peak at 1600 cm^{-1} assigned to C═C stretching vibration of skeleton as a reference) compared to those of GN-MDI. This indicates that ODA was successfully grafted onto the GN-MDI surface. Note that excess MDI and ODA were required in the series of modification reactions to avoid tethers between GN. The final filtrate in the purification process was colorless (Supporting Information, Figure S2). The corresponding FTIR spectrum was nearly identical to that of neat DMF, and the absorption at 1225 cm^{-1} for the C−O−C stretch of ODA was not detected (Supporting Information, Figure S2), indicating that the filtrate was free of ODA.

To confirm the reactivity of grafted amino groups, both the as-prepared MG and BPADA were added into DMF for reaction, and the resulting solids (MG-BPADA) were subjected to the same thermal imidization. Compared to MG, the characteristic bands at 1778 and 1720 cm^{-1} (Supporting Information, Figure S3a) are apparent and are assigned to the asymmetric and symmetric stretching vibrations of imide C═O. Furthermore, the bands at ∼2960 and 2870 cm^{-1} are also observed (Supporting Information, Figure S3b), and these are attributed to the asymmetric C−H stretch of methyl groups from BPADA. Thus, it is concluded that NH_2 of SMS can be highly reactive, providing a feasible starting platform to fabricate MG/PI nanocomposites via polymer grafting. In addition, the results indirectly demonstrate that the thermal stability of SMS on the MG surface can be sufficient to survive the thermal imidization, a crucial factor for achieving the desired interface in the matrix.

The dispersion and stability of MG were directly tested in solvent due to the insolubility of graphene and its derivatives.[2,4] Note that DMF was employed as the solvent for the preparation of MG/PAA solutions. MG can be evenly dispersed in DMF solvent, and the dispersion remains stable after 2 days without any agglomerates at the bottom of the vial (Supporting Information, Figure S4). However, the GN dispersion did not retain stability indefinitely, though it was prepared by the classic chemical reduction, employing hydrazine hydrate and SDBS surfactant. Thus, the chemical modification of GN with SMS containing NH_2 was essential to achieve a homogeneous and stable dispersion, which in turn was required for fabricating the MG/PI nanocomposites via *in situ* polymerization.

To quantify the extent of SMS grafting, TGA measurements were conducted and the results are presented in Figure 3.

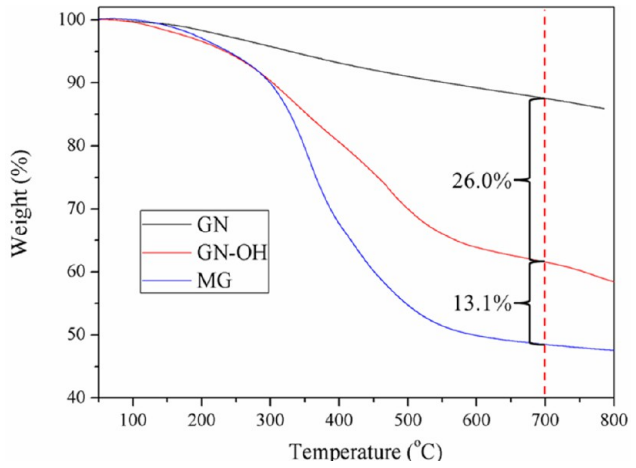

Figure 3. TGA curves of GN before and after surface modification: GN, GN-OH, and MG.

Compared to GN, 26.0 wt % grafting is observed in GN-OH after diazonium addition. The latter process provides a mass of reactive sites for further reactions, and a further weight loss of 13.1 wt % is observed. The total weight loss due to SMS decomposition is ~39.1 wt %, indicating that the loading of SMS containing NH_2 on the MG surface was ~39.1 wt %. Because of the high residual chars of ODA and MDI during thermal decomposition, the mass loss of GN-OH was used to estimate the grafting density of NH_2. Assuming that hydroxyl groups on the GN-OH surface were completely reacted by MDI, one calculates a high grafting density of 1 NH_2 per 34 carbon atoms. This grafting efficiency would afford an attractive platform for polymer grafting in the following *in situ* polymerization.

High grafting efficiency and surface modification will reduce attractive interactions among MG, thereby promoting exfoliation into individual sheets.[11] To illustrate complete exfoliation of MG in DMF solvent, we obtained the AFM images of GN-OH and MG under tapping mode (Figure 4). The thickness of the individual GO is 0.77 nm, which was reported previously.[46] The thickness of MG increased to 4.03 nm via multistep reactions, and the average lateral dimension of MG decreased to ~500 nm (determined from cross-section analyses). This result matches well with other reports.[11,15] Note that the sheets were seemingly uniform layers, suggesting that SMS was homogeneously grafted onto the GN surface. Grafted SMS on the MG surface can increase the probability of chain engagement, leading to increased mechanical interlocking with polymer chains.[22,25] Surface modification of GN provides a convenient means to fabricate high-quality interfaces in the matrix.

To confirm the near-absence of a stacking order for MG and MG aggregation in the polymer matrix, the XRD patterns of EG, GO, MG, neat PI, and MG/PI specimens are shown in Figure 5. Compared with the strong diffraction peak of EG located at 26.5° (corresponding to an interlayer spacing of about 0.34 nm), that of GO exhibits a relatively weak diffraction

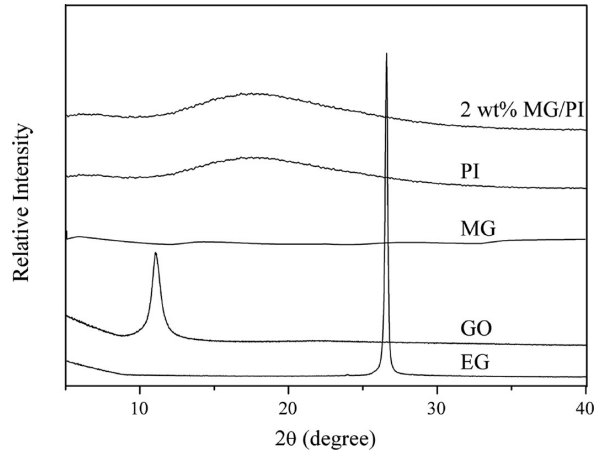

Figure 5. XRD patterns for EG, GO, MG, neat PI, and 2 wt % MG/PI specimens.

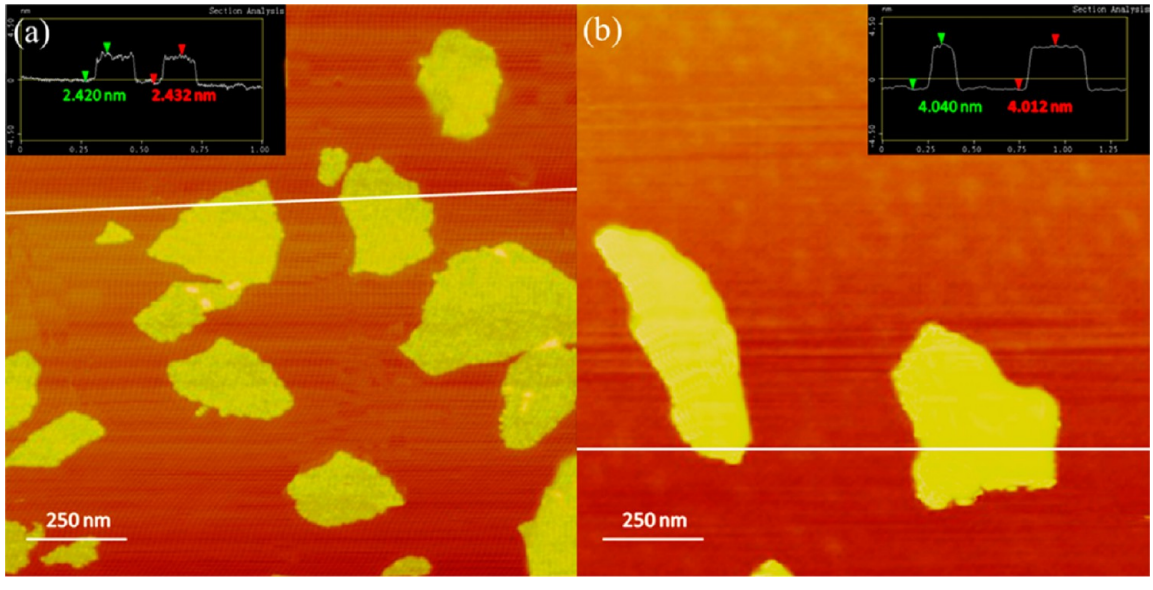

Figure 4. Typical tapping mode AFM images of (a) GN-OH and (b) MG as well as their cross-section analyses (inset), respectively.

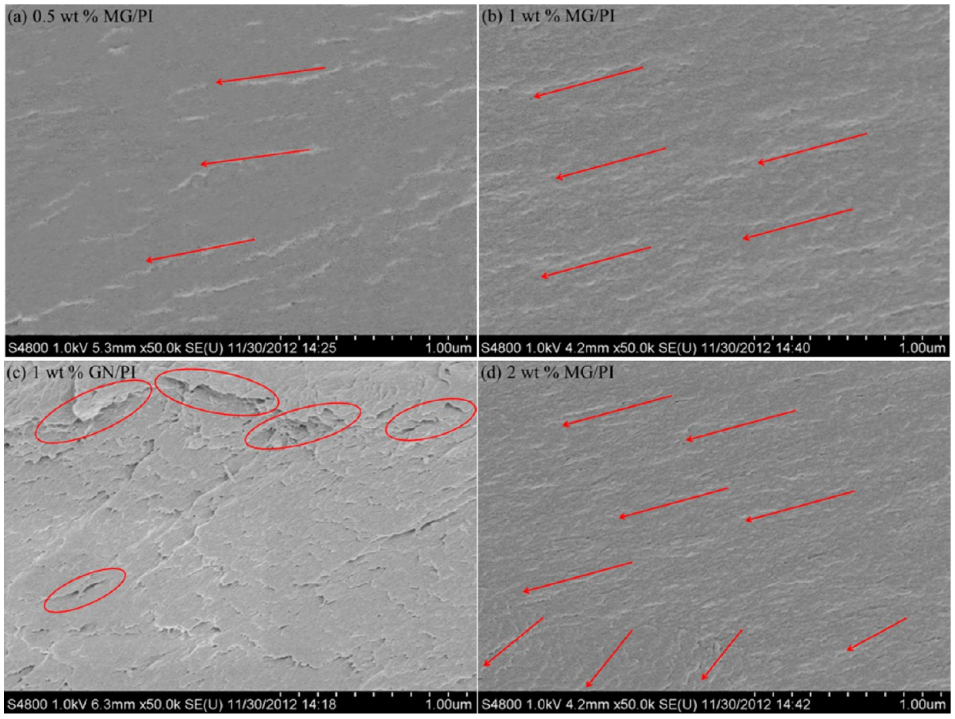

Figure 6. FESEM images of (a) 0.5 wt % MG/PI, (b) 1 wt % MG/PI, (c) 1 wt % GN/PI, and (d) 2 wt % MG/PI nanocomposites.

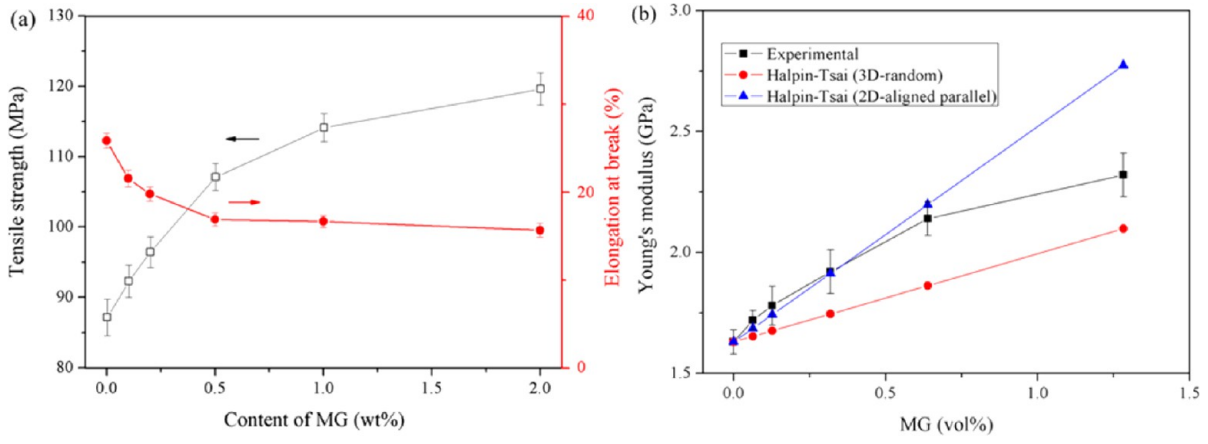

Figure 7. (a) Relationship of tensile strength and elongation at break with MG concentrations and (b) comparison between fitting results by the Halpin−Tsai model and the experimental data.

peak at 11.4°. This peak demonstrates that the interlayer spacing of GO has increased to 0.77 nm. After grafting SMS onto the GN surface, the XRD trace of MG presents no visible peak, indicating the stacking of MG is disordered.[10,47] Furthermore, the XRD patterns of neat PI and MG/PI specimens exhibit the same weak and broad diffraction peak, and no visible peak, assigned to the aggregation of MG, is observed. As suggested by Ramanathan et al.[48] and Cao et al.,[10,11,47] the dispersion of MG in the matrix is close to the single-sheet level.

3.2. Morphology of MG/PI Nanocomposites. The photograph of specimens was checked as the simplest qualitative test to observe the dispersion state of MG in the matrix.[47] Apparently, the MG/PI nanocomposite films (dog-bone type, for mechanical tests) show homogeneous appearances by visual inspection, indicating uniform distribution of MG in the PI matrix (Supporting Information, Figure S5). FESEM images of specimen cross sections were obtained to evaluate the dispersion and compatibility of GN and MG in the PI matrix. The images of the MG/PI nanocomposites show homogeneous dispersions of MG (Figure 6a,b,d). The MG tends to present as oriented colonies in the matrix (Figure 6a,b,d, marked by red arrows), especially for low MG concentrations (≤1 wt %). The observed oriented configurations are attributed to solvent evaporation induced orientation, casting induced orientation, and thickness confinement (the average thickness of films is around 50 μm whereas the lateral size of MG is larger than several hundred nanometers).[46,49] In those specimens containing lower MG contents, the effect of the above three factors is more striking due to ample adjustment space for forming oriented distributions. With increasing MG content, the adjustment of oriented distributions of MG was only partly achieved because of insufficient free volume.

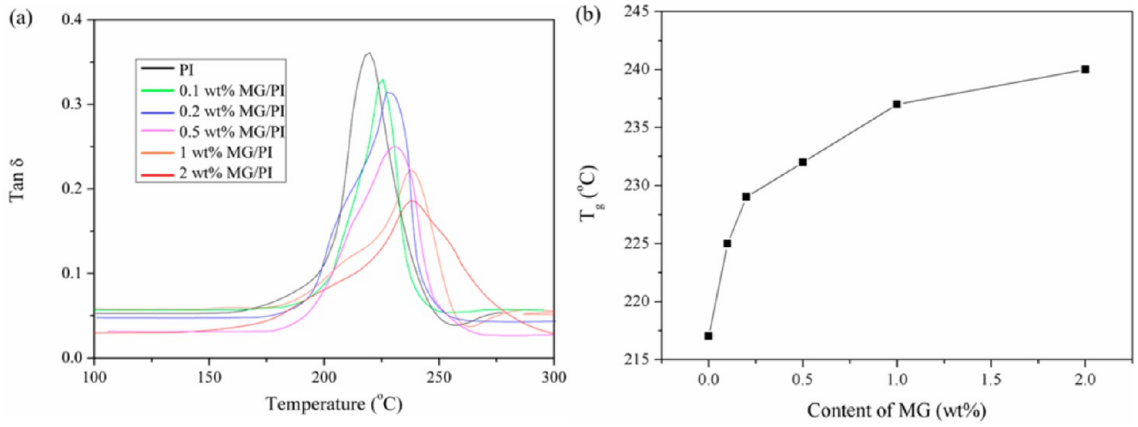

Figure 8. (a) Damping spectra of neat PI and MP/PI nanocomposite films and (b) relationship of T_g with content of MG.

The FESEM images show that MG is tightly embedded within the matrix. Furthermore, no obvious defects are observed in sections of these MG/PI nanocomposites. As discussed above, the SMS-rich surface of MG affords a platform for the construction of an interfacial layer, which prevents restacking of graphene nanosheets and ensures chemical compatibility and mechanical interlocking with the matrix. The *in situ* polymerization method typically produces a uniform dispersion of MG and strong covalent interaction. On the other hand, some cracks and agglomerations (Figure 6c, marked by red ellipses) are manifest in the 1 wt % GN/PI nanocomposite. GN tends to agglomerate because of the Van der Waals interaction between planar structures, despite the chemical reduction of GO achieved with SBDS. Nonuniform dispersions of graphene will significantly reduce its effectiveness in nanocomposites.[5,24] Fortunately, use of both chemical modification of GN and *in situ* polymerization produces the desired interface, homogeneous dispersion, good interfacial compatibility, and strong interfacial regions. These characteristics, combined with an oriented arrangement of MG to efficiently transfer stress across interfaces,[46] result in high-performance polymer/graphene nanocomposites.

3.3. Reinforcing Effect of MG. Relationships of mechanical properties with different loading amount are illustrated in Figure 7. The MG-PI nanocomposites exhibit increased tensile strength and Young's modulus. For example, the addition of only 2 wt % MG (1.28 vol%) results in a roughly 40% increase in tensile strength, from 87 to 120 MPa (for PI parallel specimen), while the Young's modulus increases by 42%. The elongation at break exhibits a slightly downward trend with increasing MG loading, although the decrease in ductility is much less than those reported in the literature.[45,50] The elongation at break (ductility) is an important parameter affecting tribological behavior.[51,52] Furthermore, the direct evidence (Supporting Information, Figure S6) indicates that the MG/PI nanocomposite film retains substantial flexibility even though the MG concentration reaches 2 wt %.

The effectiveness of reinforcing fillers used in polymer nanocomposites depends strongly on filler distribution, which can be inferred by comparing measured behavior with model predictions.[22−24] The Halpin−Tsai model has been widely used for this purpose and yields values of elastic modulus for unidirectional and randomly distributed filler-reinforced nanocomposites. The modified Halpin−Tsai equation adopted in our previous work was also used to predict values of Young's modulus for MG/PI nanocomposite films in this study.[46] All the parameters used were identical to the previous study, except for the MG dimensions (thickness, 4 nm; length, 500 nm) and the Young's modulus of neat PI (1.63 GPa). As shown in Figure 7b, the 2D-aligned model provides a much closer fit to the experimental result compared to the 3D-random model, especially for lower filler concentrations (≤1 wt %), implying that MG could be aligned parallel to the surface. The prediction of the modified Halpin−Tsai model is also consistent with the FESEM observations, indicating an oriented distribution of MG in the PI matrix. Note that the modified Halpin−Tsai model was derived assuming strong interface adhesion.[53] Thus, the observed fit indicates both MG alignment and strong interface adhesion, factors which should inhibit crack propagation.

The tensile fracture surfaces of polymer nanocomposites provide indications of the condition of the interface and the filler distribution. The neat PI film exhibits a relatively flat and smooth fracture surface (Supporting Information, Figure S7a). Aligned layered structures are evident on the tensile fracture surface, particularly for nanocomposite films with lower MG content (Supporting Information, Figure S7b,c). These observations lead us to conclude that oriented MG colonies were present as layered structures in the PI matrix. When the concentration of MG was 2 wt %, layered structures were still aligned parallel to the surface. During tensile loading, extensive matrix flow induced alignment of MG colonies along the tensile axis (elongations were >15%). The MG is tightly embedded in the matrix without apparent defects or flaws, indicating both mechanical interlocking and covalent adhesion between filler and matrix. The observed behavior can be attributed to the high quality of the interfacial layer. However, some individual GN nanosheets are exposed on the fracture surface of 1 wt % GN/PI specimen (Supporting Information, Figure S7d), reflecting poor interface between GN and the matrix. Therefore, it is evident that the strategy of the incorporation of SMS containing NH_2 can produce an effective filler−matrix interface and provide a feasible pathway for efficient load transfer.

DMA experiments were undertaken to further explore reinforcing mechanisms and the nature of the interface. Representative damping spectra (tan δ versus T) for neat PI and MG/PI nanocomposites are illustrated in Figure 8a. With increasing MG loadings, the tan δ peaks broaden and the peak heights decrease. Around the T_g region (tan δ peaks), the damping behavior is closely related to the response of polymer segments to the imposed load. Segment confinement/

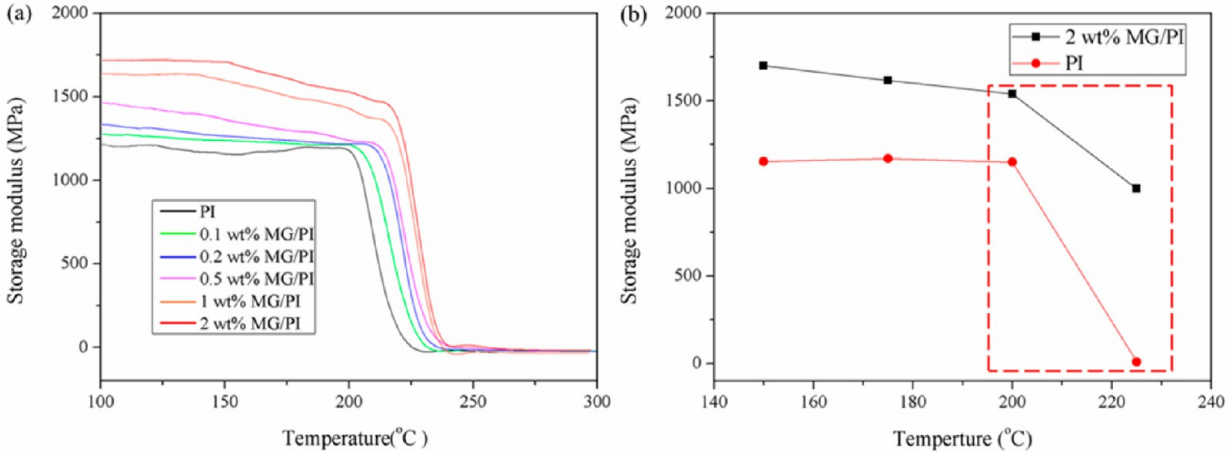

Figure 9. (a) Storage modulus of neat PI and MG/PI nanocomposite films and (b) storage modulus of neat PI and 2 wt % MG/PI nanocomposite films as a function of temperature.

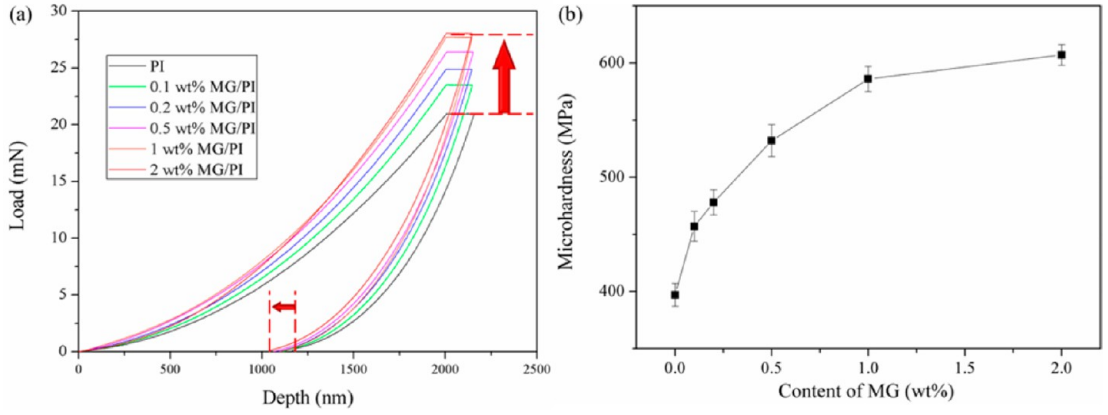

Figure 10. (a) Typical loading-hold-unloading curves and (b) microhardness of neat PI and MG/PI specimens.

restriction increases with increasing MG content due to immobilization of polymer chains near the MG surface. As a result of confinement, natural segmental motion and relaxation can only occur at higher temperatures and over a broader temperature range,[53] illustrating the two main features observed above.

The T_g values are extracted from the tan δ peaks of the damping spectra, and changes in T_g with MG content are shown in Figure 8b. The T_g value for the neat PI film (217 °C) matches with reported values.[17,18] The T_g values of MG/PI nanocomposites increase with increasing MG content, illustrating the confinement effect at interfaces. This also indicates a high grafting efficiency of PI chains on the MG surfaces,[22−24] further confirming a high grafting density of SMS containing NH_2. The grafting results in covalent adhesion between two phases, which is central to the confinement effect. An additional phenomenon comes into play during tensile loading, where mechanical unlocking can occur due to disengagement of grafted polymer chains and SMS on the MG surfaces. This structural feature is distinct from simple reactive groups grafted onto the GN surface, and the resulting phenomenon preserves some of the ductility of MG/PI nanocomposites. The GN surface modification employed here produces a strong and tough interface that provides effective stress transfer during loading. The mechanical interlocking, interfacial compatibility and covalent adhesion induced by surface modification of GN combined with oriented distribution account for the observed increases in strength.

The storage modulus of neat PI and all the MG/PI nanocomposites was plotted as a function of temperature (Figure 9a), showing that the storage modulus increased with increasing MG content. The increase is attributed to the uniform, oriented dispersion and to strong interface adhesion. The high modulus (0.25 TPa) and intrinsic strength (125 GPa) of grapheme undoubtedly contribute to the increases as well.[32] For clarity, Figure 9b shows the storage modulus for neat PI and the 2 wt % MG/PI nanocomposite versus temperature. The storage modulus of the nanocomposite film is 35−50% greater than that of neat PI at 150−200 °C. More significantly, the storage modulus of the nanocomposite is 998 MPa at 225 °C, while that of the neat PI is 10 MPa. Note that thermo-mechanical behavior is especially critical for wear-resistant materials.

Given the high modulus of MG and the oriented dispersion within MG/PI films, we expect to observe increased hardness in MG/PI specimens. Figure 10 shows typical loading-hold-unloading curves and microhardness of neat PI and MG/PI specimens. On loading, the force increases with increasing depth. The curves in Figure 10a show that resistance to indentation increases with increasing MG loading, as expected. The microhardness of MG/PI specimens in Figure 10b shows a similar dependence on MG content, although the dependence diminishes at loadings >1%, where the effect starts to saturate.

The observation is consistent with our previous work.[46] The 2 wt % MG/PI specimen shows a microhardness value 1.5-fold greater more than that of neat PI.

Because of its applications in high-tech fields, thermal stability is another key parameter for PI nanocomposites. Figure 11 shows the TGA curves of neat PI and MG/PI

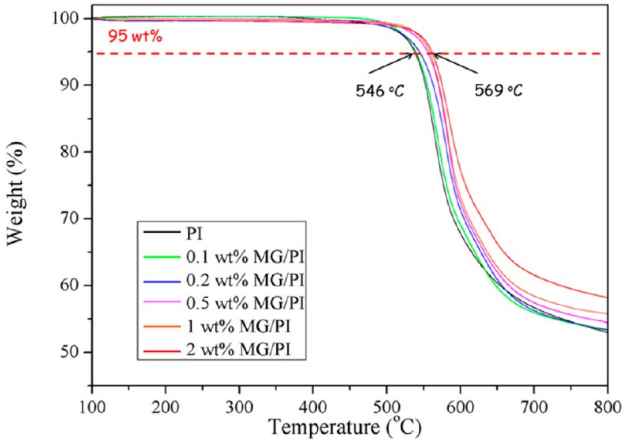

Figure 11. TGA thermograms of neat PI and MG/PI specimens.

nanocomposites. The incorporation of 2 wt % MG noticeably enhances thermal stability of PI, as the temperature for 5% weight loss of the resulting nanocomposites is shifted from 546 to 569 °C. The detailed data of other specimens was detected (Supporting Information, Table S1). It is worthy of note that the increase in thermal stability of PI nanocomposites is much greater than those reported in the literature.[17,46,49,50,54] Uniform and oriented distributions of MG and strong covalent adhesion between two phases can make full use of excellent thermal stability of MG. As Ha and co-workers suggested,[50] the carbon surface of MG in the specimens might act as a radical scavenger to delay the thermal degradation temperature and hence result in improving thermal stability of PI. Furthermore, the incorporation of SMS onto the GN surfacce can strengthen the "tortuous path" effect,[46] enhancing the thermal stability of PI. Note that there exists no obvious weight loss before 500 °C, which is different from that reported by Ha and co-workers.[50] It is ascribed to the intelligent construction of excellent thermal stability and compatibility of interface, as manifested above.

The unique conductive behavior of graphene drove us to explore the effect of MG on the conductivity of the resulting nanocomposites. The classical chemical reduction of GO can contribute to the effective recovery of the sp^2 during the preparation process of MG. However, the incorporation of SMS containing NH_2 also might increase defective parts of MG. As shown in Figure 12, there exhibits a sharp upward trend with increasing MG content. The conductivity of 0.5 wt % MG/PI nanocomposites increases remarkably from 1.5×10^{-13} to 3.1×10^{-4} S m^{-1}. When the MG content is over 0.5 wt %, the effect starts to saturate and the conductivity values of MG/PI nanocomposites are above the antistatic criterion of 10^{-6} S m^{-1}.[46] Luong et at. have reported that the electricity conductivity of the 0.75 wt % functionalized graphene/PI composite was 8.9×10^{-5} S m^{-1}.[55] Recently, Ha and co-workers have investigated the electrical conductivity of 1 wt % chemical reduced GO by three different reducing agents, and results were 2.42×10^{-4}, 8.65×10^{-3}, and 8.68×10^{-2} S m^{-1}, respectively.[50] Compared to our results, it is believed that the

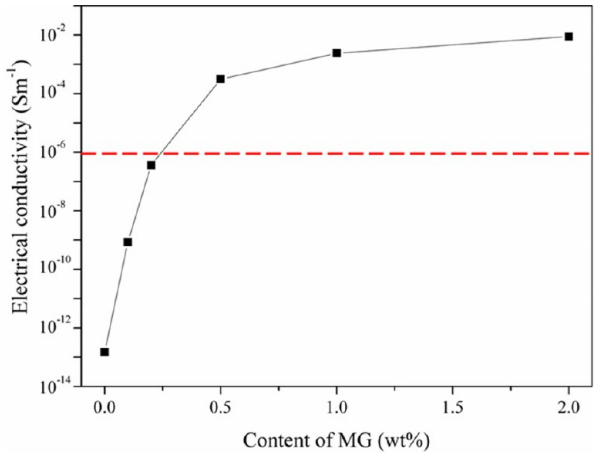

Figure 12. Electrical conductivity of neat PI and MG/PI specimens.

adopted strategy (the incorporation of SMS containing NH_2 in the matrix) might hardly increase the defective parts of MG. Furthermore, the conductivity percolation is observed at relative low MG content (about 0.5 wt %). This is ascribed to an oriented and uniform dispersion of MG in the PI matrix, generating a 2D conducting network.[46]

3.4. Tribological Effect of MG. The friction coefficient and wear rate of neat PI and MG/PI specimens were measured under a load of 6 N at a frequency of 300 Hz, as shown in Figure 13. The wear exhibits a continuous downward trend

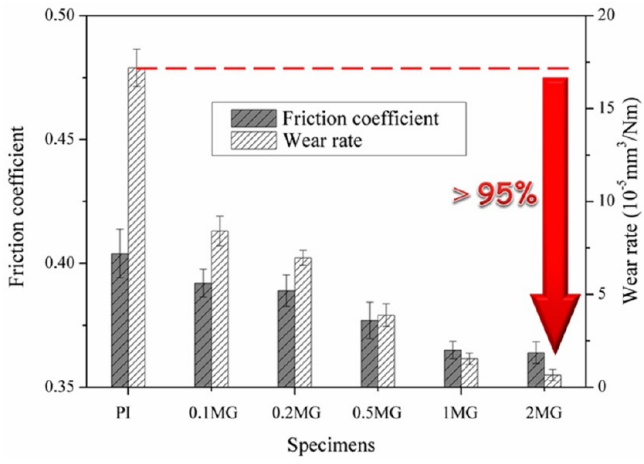

Figure 13. Friction coefficient and wear rate of neat PI and MG/PI specimens.

after the incorporation of MG (from 0.1–2 wt %). What is more, the wear rate of 2 wt % MG/PI specimen (0.66×10^{-5} mm^3/N m) is reduced by >95% in comparison with that of neat PI. In other words, the wear resistance of 2 wt % MG/PI specimen is enhanced more than 20-fold. To make the point more directly, one can see clearly in Figure 14 that the wear width is reduced from 0.66 to 0.20 mm with the incorporation of 2 wt % MG. The trend in wear rate is consistent with that of wear width. Though some studies have shown moderate improvements (one or two times) in wear resistance of graphene/polymer nanocomposites, the dramatic increase in wear resistance observed here has not been reported before.[38−42] Furthermore, the incorporation of MG reduces the friction coefficient of the resulting MG/PI specimens from

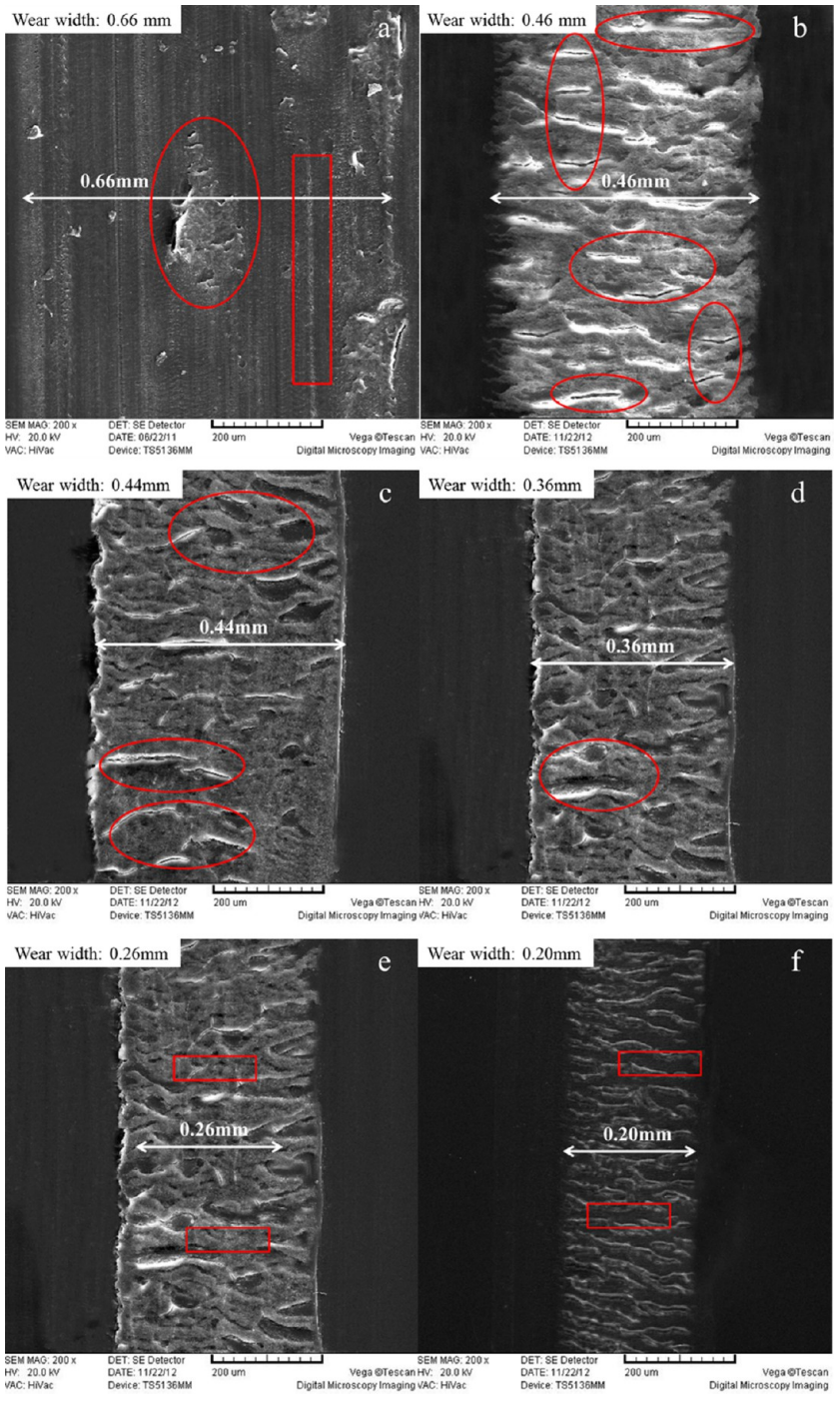

Figure 14. SEM images of worn surfaces of (a) neat PI, (b) 0.1 wt % MG/PI, (c) 0.2 wt % MG/PI, (d) 0.5 wt % MG/PI, (e) 1 wt % MG/PI, and (f) 2 wt % MG/PI specimens (magnification: 200).

0.41 to 0.36. Overall, the incorporation of MG greatly improves the tribological properties of PI nanocomposites.

SEM observations of worn surface and wear debris can be beneficial to explore the related friction and wear mechanism. Neat PI wear surface is relatively flat and displays signs of adhesive and abrasive wear (Figure 14a, marked by a red ellipse and rectangle, respectively). In contrast, worn surfaces of MG/PI specimens show some typical fatigue deformations and deep furrows (Figure 14b−f, marked by red ellipses), indicating that the type of wear changed from adhesion and abrasive wear into fatigue wear. With increasing MG content, fatigue wear is inhibited, resulting in relatively smoother and flatter worn surfaces (Figure 14e,f, marked by red rectangles). The SEM images of wear debris of neat PI and MG/PI specimens are given in Figure 15, showing a shift in the morphology of wear debris from large platelets to small particles after the incorporation of MG. Furthermore, the size of wear debris decreased with increasing MG content. With regard to the relationship between debris size and wear rate, the debris size is consistent with the wear resistance of the corresponding specimen.

The tribological properties of a material depend on multiple factors, including interfacial adhesion, dispersion of filler, chain segment structure, mechanical properties, hardness, processing

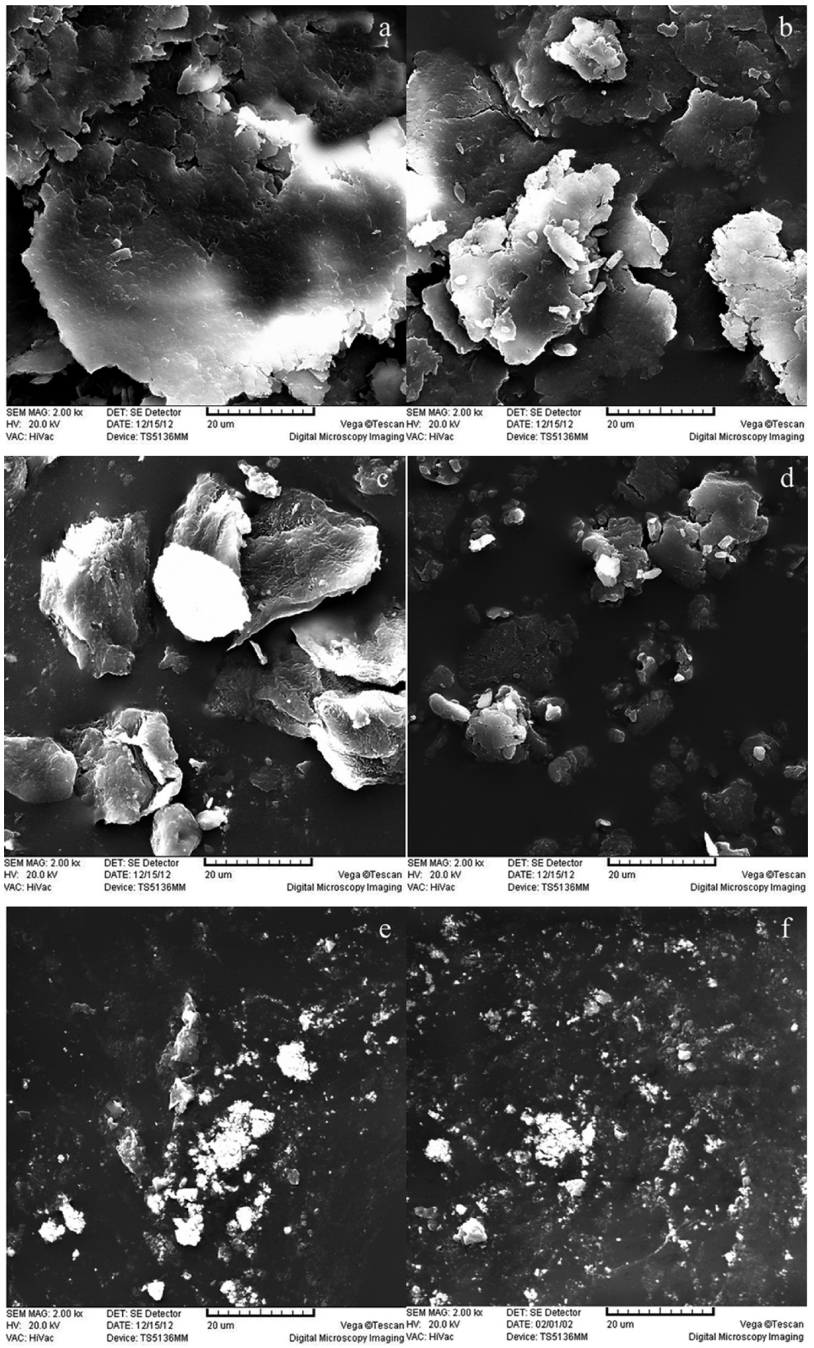

Figure 15. SEM images of wear debris of (a) neat PI, (b) 0.1 wt % MG/PI, (c) 0.2 wt % MG/PI, (d) 0.5 wt % MG/PI, (e) 1 wt % MG/PI, and (f) 2 wt % MG/PI specimens (magnification: 2000).

technology, surface tension, etc.[56−60] The observed increase in wear resistance is attributed to two aspects: (a) tribological effects of MG that, including protective effect and suppression effect, and (b) the increase in mechanical properties.

A simplified schematic diagram provides an explanation for the improved wear resistance imparted by tribological effects of MG (Figure 16a,b). As shown in Figure 16b, the bands at 1330 and 1595 cm^{-1} arise in Raman spectra of worn surfaces of the 2 wt % MG/PI specimen. From these two characteristic bands of MG (Supporting Information, Figure S8), the difference demonstrates that MG exists on the worn surface of 2 wt % MG/PI nanocomposites. On one hand, the appearance of MG on the worn surface provides direct evidence of the protective effect against the external force. Furthermore, we assert that the MG constraint of proximal polymer chains in the matrix plays a role to mitigate frictional forces due to the two-dimensional nature and oriented distribution in the matrix. Strong interface interaction between MG and matrix can also strengthen the protective effect against the friction force. On the other hand, the MG filler reduces wear rates by reducing the debris size.[36,61−63] The large interfacial contact area of MG effectively interferes with and suppresses the generation of wear debris. This suppression effect can obviously prevent the generation of sheet-like wear debris, therefore leading to reduce wear.

As discussed above, MG/PI specimens exhibit attractive enhancements in properties, including higher tensile strength,

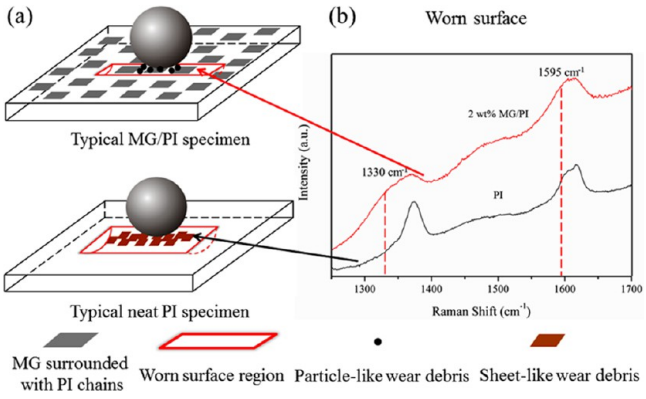

Figure 16. (a) Typical proposed model for the friction and wear mechanism of neat PI and MG/PI specimens. (b) Raman spectra of worn surface of neat PI and 2 wt % MG/PI specimens.

Young's modulus, microhardness, resistance to indentation, T_g, and thermo-mechanical properties. These enhancements can also lead to increased wear resistance.[56,58,61,62] The temperature of worn surfaces typically increases from frictional heating during testing. As shown in Figure 10, MG/PI specimens retain higher storage modulus values compared to neat PI, even at high temperatures (200−230 °C), effectively enhancing wear resistance. During sliding wear, increased strength/hardness can greatly reduce deformations and fragmentations of MG/PI specimens, increasing wear resistance. More importantly, specimens with superior mechanical properties can be more difficult to ablate, according to Ratner-Lancaster.[51,52] Consequently, the huge improvement in wear resistance can be achieved.

In this work, both normal load and sliding velocity were constant. The friction force depends by definition on the product of real contact area and shear strength.[18] After the incorporation of MG, an integrated effect of increased tensile strength, Young's modulus, microhardness, and resistance to indentation limits deformation of the worn surface (Figure 14a,f) and thus reduces the real contact area. Though the shear strength of the two specimens differs, there exists a significant possibility that the friction force would decreases if the real contact area plays a determining role. Accordingly, the large reduction in the real contact area contributes to the observed decrease in the friction coefficient for MG/PI specimens. Furthermore, the change in the morphology of wear debris particles may provide additional insight. Particle-like wear debris may effectively roll on the worn surface, reducing the friction coefficient (Figure 16a). In addition, the sliding of individual graphene planes within few-layered graphene platelets might function as a solid lubricant,[30,36] further reducing the friction coefficient.

Through the comparison between 1 wt % GN/PI and 1 wt % MG/PI specimens (Table 1), we can further illustrate the effect of the surface modification of GN. The thermal stability, electrical conductivity, and mechanical and tribological properties of 1 wt % MG/PI specimen are clearly superior to those of the 1 wt % GN/PI specimen. This illustrates that the oriented and uniform dispersion of MG plays a critical role in the improvement of electrical conductivity by a comparison between 1 wt % MG/PI and 1 wt % GN/PI specimens. Compared to neat PI, the wear rate of 1 wt % GN/PI specimen is slightly less, while the friction coefficient is greater. This is attributed to the poor GN-matrix adhesion, which facilitates

Table 1. Data Based on Properties of 1 wt % MG/PI and 1 wt % GN/PI Specimens

specimens	1 wt % MG/PI	1 wt % GN/PI
tensile strength (MPa)	115	86
Young's modulus (GPa)	2.14	1.76
elongation at break (%)	16.67	7.83
T_g (°C)	237	221
T_5[a] (°C)	567	551
electricity conductivity (S m^{1-})	2.6×10^{-3}	1.8×10^{-4}
friction coefficient	0.365	0.463
wear rate (mm^3/N m)	1.54×10^{-5}	8.36×10^{-5}

[a]T_5, the temperature at 5 wt % of weight loss was recorded by TGA with a heating of 20 °C/min under N_2 atmosphere.

GN exfoliation, generating wear debris. Wear debris containing exposed GN acts as abrasive particles between the specimen and ball, increasing surface roughness and degrading tribological properties. The strong matrix-MG interface interaction inhibits MG exfoliation.[18] Intelligent design and construction of the MG-matrix interface enhances the resulting properties of the nanocomposites.

In addition, it might be interesting to compare the reinforcing and tribological effects of MG with that of their 1D counterparts, CNTs. Since the effectiveness of MG and CNTs is suggested to be the matrix dependent,[19,64−66] the interesting discussion is focused specifically on their PI composites. Satyanarayana and co-workers have reported that the addition of 0.5 wt % SWCNTs yielded a 2-fold increase in the wear life.[19] Liu and co-workers have investigated tribological properties of MWCNTs/PI nanocomposites, and results showed that the incorporation of 5 wt % MWCNTs only provided a 1-fold increase in wear resistance under the optimum friction testing condition.[64] In this work, it is believed that the 20-fold increase in wear resistance of the 2 wt % MG/PI specimen can illustrate the superior tribological effect of MG, though the friction testing condition exists slightly different. On the other hand, Yuen et al. have prepared acid and amine modified MWCNTs/PI composites and results showed that the 1 wt % acid-modified MWCNTs only afforded a 7.8% increase in tensile strength and 1 wt % amine-modified MWCNTs only provided a 20% increase in tensile strength.[65] Qunaies and co-workers reported that the addition of 0.5 vol % SWCNTs into the PI matrix yielded an increased electrical conductivity (3×10^{-5} S m^{1-}).[66] As mentioned above, the obtained tensile strength and electrical conductivity of MG/PI specimens may illustrate the excellent reinforcing effect of MG.

4. CONCLUSIONS

Graphene can be an effective wear-resistant filler in the polymer matrix through proper interface design and construction. In this study, such interfaces were designed and produced in MG/PI nanocomposites by the surface modification of SMS containing NH_2 onto the GN surface, followed by *in situ* polymerization. The resulting interface produced efficient stress transfer across the interface and enhanced the properties of the nanocomposites. For the reinforcing aspect, the incorporation of 2 wt % MG produced a ~40% increase in tensile strength, 42% increase in Young's modulus, 53% increase in microhardness, ~23 °C increase in T_g, and ~23 °C increase in T_5. The storage modulus of 2 wt % MG/PI nanocomposites was 998 MPa at 225 °C, while that of the neat PI was 10 MPa. The electrical percolation threshold is observed at only 0.5 wt % MG in this

composite system. For the tribological aspect, the same nanocomposites showed a 20-fold increase in wear resistance and a 12% reduction in friction coefficient. The superior wear resistance is attributed to the increase in mechanical properties, suppression effect of MG in the generation of wear debris, and protective effect of MG against the friction force.

■ ASSOCIATED CONTENT

Supporting Information

More information about schematic diagram of the contact configuration of the reciprocating friction and wear testing machine; additional FTIR spectra of ODA, last filtrate, pure DMF, and MG-BPADA (after thermal imidization); dispersibility and time-dependent stability of GO, GN, and MG in DMF solvent; appearance for dog-bone type specimens of neat PI and MG/PI nanocomposite films; a typical figure illustrating high flexibility of MG/PI nanocomposite film; SEM micrographs of fracture surfaces of neat PI, GN/PI, and MG/PI specimens; Raman spectra of MG and data based on properties of all the MG/PI specimens. This material is available free of charge via the Internet at http://pubs.acs.org.

■ AUTHOR INFORMATION

Corresponding Author

*E-mail: lits@fudan.edu.cn. Fax: +86-21-51630401.

Notes

The authors declare no competing financial interest.

■ ACKNOWLEDGMENTS

We acknowledge financial support from National Basic Research Program of China (Grant 2011CB605704).

■ REFERENCES

(1) Novoselov, K. S.; Geim, A. K.; Morozov, S. V.; Jiang, D.; Zhang, Y.; Dubonos, S. V.; Grigorieva, I. V.; Firsov, A. A. *Science* **2004**, *306*, 666−669.
(2) Alison, Y. W. S.; Shannon, M. N. *Soft Matter* **2013**, DOI: 10.1039/C3SM00092C.
(3) Lee, S. K.; Rana, K.; Ahn, J. H. *J. Phys. Chem. Lett.* **2013**, *4*, 831−841.
(4) Chen, J.; Li, C.; Shi, G. Q. *J. Phys. Chem. Lett.* **2013**, *4*, 1244−1253.
(5) Huang, X.; Qi, X. Y.; Boey, F.; Zhang, H. *Chem. Soc. Rev.* **2012**, *41*, 666−686.
(6) Das, S.; Wajid, A. S.; Shelburne, J. L.; Liao, Y.-C.; Green, M. J. *ACS Appl. Mater. Interfaces* **2011**, *3*, 1844−1851.
(7) Rafiq, R.; Cai, D. Y.; Jin, J.; Song, M. *Carbon* **2010**, *48*, 4309−4314.
(8) Satti, A.; Larpent, P.; Gun'ko, Y. *Carbon* **2010**, *48*, 3376−3381.
(9) Yoonessi, M.; Gaier, J. R. *ACS Nano* **2010**, *4*, 7211−7220.
(10) Cao, Y. W.; Feng, J. C.; Wu, P. Y. *Carbon* **2010**, *48*, 3834−3839.
(11) Cao, Y. W.; Feng, J. C.; Wu, P. Y. *Carbon* **2010**, *48*, 1683−1685.
(12) Yoonessi, M.; Shi, Y.; Scheiman, D. A.; Lebron-Colon, M.; Tigelaar, D. M.; Weiss, R. A.; Meador, M. A. *ACS Nano* **2012**, *6*, 7644−7655.
(13) Son, D. L.; Kim, T. W.; Shim, J. H.; Jung, J. H.; Lee, D. U.; Lee, J. M.; Park, W. I.; Choi, W. K. *Nano Lett.* **2010**, *10*, 2441−2447.
(14) Wang, X.; Hu, Y.; Song, L.; Yang, H. Y.; Xing, W. Y.; Lu, H. D. *J. Mater. Chem.* **2011**, *21*, 4222−4227.
(15) Fang, M.; Wang, K. G.; Lu, H. B.; Yang, Y. L.; Nutt, S. *J. Mater. Chem.* **2009**, *19*, 7098−7105.
(16) Wilson, D.; Stenzenberger, H. D.; Hergenrother, P. M. *Polyimides*; Chapman & Hall: London, 1990.
(17) Huang, T.; Liu, P.; Lu, R. G.; Huang, Z. Y.; Chen, H. M.; Li, T. S. *Wear* **2012**, *292*−*293*, 25−32.
(18) Samyn, P.; Schoukens, G.; Verpoort, F.; Craenenbroeck, J. V.; Baets, P. D. *Macromol. Mater. Eng.* **2007**, *292*, 523−556.
(19) Satyanarayana, N.; Rajan, K. S. S.; Sinha, S. K.; Shen, L. *Tribol. Lett.* **2007**, *27*, 181−188.
(20) Wang, Y. W.; Chen, W. C. *Mater. Chem. Phys.* **2011**, *126*, 24−30.
(21) Ge, J. J.; Zhang, D.; Li, Q.; Hou, H. Q.; Graham, M. J.; Dai, L. M.; Harris, F. W.; Cheng, S. Z. D. *J. Am. Chem. Soc.* **2005**, *127*, 9984−9985.
(22) Mamedov, A. A.; Kotov, N. A.; Prato, M.; Guldi, D. M.; Wicksted, J. P.; Hirsch, A. *Nat. Mater.* **2002**, *1*, 190−194.
(23) Liu, J. Q.; Tang, J. G.; Gooding, J. J. *J. Mater. Chem.* **2012**, *22*, 12435−12452.
(24) Cai, D. Y.; Song, M. *J. Mater. Chem.* **2010**, *20*, 7906−7915.
(25) Salavagione, H. J.; Martínez, G.; Ellis, G. *Macromol. Rapid Commun.* **2011**, *32*, 1771−1789.
(26) Qu, L. W.; Lin, Y.; Hill, D. E.; Zhou, B.; Wang, W.; Sun, X. F.; Kitaygorodskiy, A.; Suarez, M.; Connell, J. W.; Allard, L. F.; Sun, Y. P. *Macromolecules* **2004**, *37*, 6055−6060.
(27) Lebrón-Colón, M.; Meador, M. A.; Gaier, J. R.; Solá, F.; Scheiman, D. A.; McCorkle, L. S. *ACS Appl. Mater. Interfaces* **2010**, *2*, 669−676.
(28) Leu, C. M.; Wu, Z. W.; Wei, K. H. *Chem. Mater.* **2002**, *14*, 3016−3021.
(29) Amanov, A.; Cho, I. S.; Pyoun, Y. S.; Lee, C. S.; Park, I. G. *Wear* **2012**, *286*−*287*, 136−144.
(30) Berman, D.; Erdemir, A.; Sumant, A. V. *Carbon* **2012**, *54*, 454−459.
(31) Smolyanitsky, A.; Killgore, J. P.; Tewary, V. K. *Phys. Rev. B* **2012**, *85*, 035412(1−6).
(32) Young, R. J.; Kinloch, I. A.; Gong, L.; Novoselov, K. S. *Compos. Sci. Technol.* **2012**, *72*, 1459−1476.
(33) Deng, Z.; Smolyanitsky, A.; Li, Q. Y.; Feng, X. Q.; Cannara, R. J. *Nat. Mater.* **2012**, *11*, 1032−1037.
(34) Shin, Y. J.; Stromberg, R.; Nay, R.; Huang, H.; Wee, A. T. S.; Yang, H.; Bhatia, C. S. *Carbon* **2011**, *49*, 4070−4073.
(35) Kim, K. S.; Lee, H. J.; Lee, C. G.; Lee, S. K.; Jang, H.; Ahn, J. H.; Kim, J. H.; Lee, H. J. *ACS Nano* **2011**, *5*, 5107−5114.
(36) Kandanur, S. S.; Rafiee, M. A.; Yavari, F.; Schrameyer, M.; Yu, Z. Z.; Blanchet, T. A.; Koratkar, N. *Carbon* **2012**, *50*, 3178−3183.
(37) Song, H. J.; Jia, X. H.; Li, N.; Yang, X. F.; Tang, H. *J. Mater. Chem.* **2012**, *22*, 895−902.
(38) Pan, B. L.; Zhang, S. P.; Li, W. Z.; Zhao, J.; Liu, J. L.; Zhang, Y. Q.; Zhang, Y. Z. *Wear* **2012**, *294*−*295*, 395−401.
(39) Liu, H.; Li, Y. Q.; Wang, T. M.; Wang, Q. H. *J. Mater. Sci.* **2012**, *47*, 1867−1874.
(40) Tai, Z. X.; Chen, Y. F.; An, Y. F.; Yan, X. B.; Xue, Q. J. *Tribol. Lett.* **2012**, *46*, 55−63.
(41) Li, Y. Q.; Wang, Q. H.; Wang, T. M.; Pan, G. Q. *J. Mater. Sci.* **2012**, *47*, 730−738.
(42) Song, H. J.; Li, N.; Li, Y. J.; Min, C. Y.; Wang, Z. *J. Mater. Sci.* **2012**, *47*, 6436−6443.
(43) Oliver, W. C.; Pharr, G. M. *J. Mater. Res.* **1992**, *7*, 1564−1583.
(44) Oliver, W. C.; Pharr, G. M. *J. Mater. Res.* **2004**, *19*, 3−19.
(45) Wang, J. Y.; Yang, S. Y.; Huang, Y. L.; Tien, H. W.; Chin, W. K.; Ma, C. C. M. *J. Mater. Chem.* **2011**, *21*, 13569−13575.
(46) Huang, T.; Lu, R. G.; Su, C.; Wang, H. N.; Guo, Z.; Liu, P.; Huang, Z. Y.; Chen, H. M.; Li, T. S. *ACS Appl. Mater. Interfaces* **2012**, *4*, 2699−2708.
(47) Cao, Y. W.; Lai, Z. L.; Feng, J. C.; Wu, P. Y. *J. Mater. Chem.* **2011**, *21*, 9271−9278.
(48) Ramanathan, T.; Abdala, A. A.; Stankovich, S.; Dikin, D. A.; Herrera-Alonso, M.; Piner, R. D.; Adamson, D. H.; Schniepp, H. C.; Chen, X.; Ruoff, R. S.; Nguyen, S. T.; Aksay, I. A.; Prud'homme, R. K.; Brinson, L. C. *Nat. Nanotechnol.* **2008**, *3*, 327.
(49) Chen, D.; Zhu, H.; Liu, T. X. *ACS Appl. Mater. Interfaces* **2010**, *2*, 3702−3708.
(50) Ha, H. W.; Choudhury, A.; Kamal, T.; Kim, D. H.; Park, S. Y. *ACS Appl. Mater. Interfaces* **2012**, *4*, 4623−4630.

(51) Stachowiak, G. W.; Batchelor, A. W. *Engineering Tribology*; Elsevier Butterworth Heinemann: Amsterdam, The Netherlands, 2005.
(52) Hutchings, I. M. *Tribology: Friction and Wear of Engineering Materials*; Elsevier Limited: London, 1992.
(53) Chen, Z. X.; Lu, H. B. *J. Mater. Chem.* **2012**, *22*, 12479−12490.
(54) Zhang, L. B.; Wang, J. Q.; Wang, H. G.; Xu, Y.; Wang, Z. F.; Li, Z. P.; Mi, Y. J.; Yang, S. R. *Composites, Part A* **2012**, *43*, 1537−1545.
(55) Luong, N. D.; Hippi, U.; Korhonen, J. T.; Soininen, A. J.; Ruokolainen, J.; Johansson, L. S.; Nam, J. D.; Sinh, L. H.; Seppälä, J. *Polymer* **2011**, *52*, 5237−5242.
(56) Huang, T.; Lu, R. G.; Wang, H. Y.; Ma, Y. N.; Tian, J. S.; Li, T. S. *J. Macromol. Sci. B* **2011**, *50*, 1235−1248.
(57) Brostow, W.; Lobland, H. H. E.; Narkis, M. *J. Mater. Res.* **2006**, *21*, 2422−2428.
(58) Brostow, W.; Deborde, J. L.; Jaklewicz, M.; Olszynski, P. *J. Mater. Educ.* **2003**, *25*, 119−132.
(59) Samad, M. A.; Sinha, S. K. *Wear* **2011**, *270*, 395−402.
(60) Loy, X. Z. K.; Sinha, S. K. *Wear* **2012**, *296*, 681−692.
(61) Wang, H. Y.; Lu, R. G.; Huang, T.; Ma, Y. N.; Cong, P. H.; Li, T. S. *Mater. Sci. Eng., A* **2011**, *528*, 6878−6886.
(62) Liu, P.; Lu, R. G.; Huang, T.; Cong, P. H.; Jiang, S. S.; Li, T. S. *Wear* **2012**, *289*, 65−72.
(63) Blanchet, T. A.; Kennedy, F. E. *Wear* **1992**, *153*, 229−243.
(64) Liu, H.; Wang, T. M.; Wang, Q. H. *Polym.-Plast. Technol.* **2012**, *51*, 1−5.
(65) Yuen, S. M.; Ma, C. C. M.; Lin, Y. Y.; Kuan, H. C. *Compos. Sci. Technol.* **2007**, *67*, 2564−2573.
(66) Qunaies, Z.; Park, C.; Wise, K. E.; Siochi, E. J.; Harrison, J. S. *Compos. Sci. Technol.* **2003**, *63*, 1637−1646.